Trapping and near-trapping by arrays of porous cylinders in water waves using the addition theorem and superposition technique

Yi-Jhou Lin [1*], Ying-Te Lee [1], Jia-Wei Lee [1] and Jeng-Tzong Chen [1,2]

[1]Department of Harbor and River Engineering, National Taiwan Ocean University, Keelung, Taiwan
[2]Department of Mechanical and Mechatronics Engineering, National Taiwan Ocean University, Keelung, Taiwan

Abstract

Following the successful experiences of solving water-wave scattering problems for multiple impermeable cylinders, we extend the null-field integral formulation to deal with the problems of surface-piercing porous cylinders in this paper. The null-field integral equations in conjunction with the addition theorem and Fourier series are employed to solve the water-wave problem. In the implementation, the null-field point can be exactly located on the real boundary free of calculating the Cauchy and Hadamard principal values thanks to the introduction of degenerate kernels for fundamental solutions. This method can be seen as a semi-analytical approach since errors attribute from the truncation of Fourier series. Not only a systematic approach is proposed but also the effect on the near-trapped modes due to porous cylinders and disorder of layout is examined. It is found that the disorder is more sensitive to suppress the occurrence of near-trapped modes than the porosity. The free-surface elevation is consistent with the results of William and Li and those by using the conventional BEM. Besides, the numerical results of the force on the surface of cylinders agree well with those in the literature.

Keywords：addition theorem, null-field integral equation, Fourier series, trapped mode, porous

1、 Introduction

A general problem in offshore engineering is to determine the wave loading exerted upon a circular cylinder. For a single cylinder, an analytical solution was available by MacCamy and Fuchs [1]. For the general case, we always resort to semi-analytical or numerical solutions. A semi-analytical solution using the wave function expansion was obtained by Spring and Monkmeyer [2] for the diffraction of linear waves by arrays of cylinders. Later, the interaction of water waves with arrays of circular cylinders was studied by Linton and Evans [3] in a similar way of Twersky approach. Linton and Evans [3] extended this approach to calculate the force in a more neat form. However, the convergence behavior of the null-field integral equation approach is superior to that of Linton and Evans method. For the boundary integral solution, it converges to L_2 energy sense in an exponential order. It is noted that we can deal with other shape of cross section in our approach, if the degenerate kernels corresponding to the special geometry are available. For example, degenerate kernel for the ellipse can be found in the book of Morse and Feshbach [4]. Also, the work of the elliptic case using the method of Linton and Evans is given in the Martin's book [5], and the numerical results are implemented by Chatjigeorgiou and Mavrakos [6]. On the other hand, some formulae are not found in the mathematical handbook or were not derived by mathematicians for the special geometry. That is to say, we have a challenging work in deriving the degenerate kernel for a special geometry case. Besides, our approach can be applied to problems containing both circular and elliptical cylinders since we introduce adaptive coordinate system and vector decomposition. For the Linton and Evans approach, it may have difficulty in their formulation since the addition theorem for translating the polar coordinates to the elliptical coordinates and vice versa is not available to the authors' best knowledge. Simply speaking, the addition theorem is not available to transform Bessel to Mathieu functions

* Corresponding author. Tel.: +886 2 24622192x6177; fax: +886 2 24632375.
E-mail addresses:M96520007@mail.ntou.edu.tw (Y.J. Lin)

when a problem contains circle and ellipse together.

Regarding numerical methods, Au and Brebbia [7, 8] employed the boundary element method (BEM) to calculate the elevation of free surface as well as the resultant force by using constant, linear and quadratic elements. By descretizing the boundary in a more genius way, Zhu and Moule [9] obtained a more accurate result. Chen [10] used the composite BEM to determine the free-surface elevation for the porous cylinders. Besides, Chen et al. [11] employed the null-field integral equation approach to study the near-trapped mode. To determine the singular integrals is a critical issue in the boundary integral equation method (BIEM). The present paper is based on the null-field BIEM while the singular integrals are transformed to series sum free of principal-value calculation using bump contour.

Localized oscillations in unbounded media are always referred to trapped modes in different contexts. For example, acoustic resonance, array-guided surface waves, edge waves, Rayleigh-Bloch waves and bound states are similar physical phenomena. Energy in the guided area is stored and can not radiate to infinity in the case of trap wave number. Water wave diffraction and near trapping by a multi-column structure was studied by Evans and Poretr [12]. Near-trapped modes were found for four, five and six cylinders. The wave number to excite the trapped modes was determined numerically by detecting the value of ka which results in the maximum force. Dirichelet and Neumann trapped modes of large number of cylinders (100) in an infinite domain were found to approach those of infinite number of cylinders by Maniar and Newman [13]. Real and absolute values for the free-surface elevation were investigated by Evans and Porter [14]. Trapped modes for a semi-infinite domain was studied by Thompson et al. [15]. For multiple cylinders in a channel, trapped modes were also found by Evans and Porter [14]. Mathematically speaking, the array-guided cylinders may result in non-trivial solutions of the homogeneous problem at particular values of wave number. It can be understood as eigenvectors corresponding to eigenvalues of certain differential operators on unbounded domains even though there is no characteristic length as mentioned by Linton and McIver [16].

Duclos and Clèment [17] extended to consider arrays of unevenly spaced cylinders, displaced randomly from a regular array according to a disorder parameter. They focused on two effects of this spacing irregularity, reduction of peak forces associated to trapped mode phenomena, and regularization of the transmission coefficient for waves propagating through the arrays. However, Duclos and Clèment [17] only considered the impermeable cylinders. On the other hand, Willams and Li [18] calculated the free-surface elevation and force for the porous cylinders. Nevertheless, they did not consider the disorder effect. We may wonder what happen for the near-trapped modes if we simultaneously consider the porous cylinder with a disorder. The effect of porosity parameter on the free-surface elevation, force and near-trapped modes will be examined. Also, the reduction of force in the case of near-trapped mode due to disorder is also our interest.

In this paper, the hydrodynamics of circular porous cylinders is studied by using the null-field integral equation in conjunction with the addition theorem and the Fourier series. The main difference between the present approach and Linton-Evans method is that we use the BIE instead of the wave function expansion. The unknown coefficient here is the Fourier coefficient on the boundary instead of weighting of wave expansion for the domain. The wave interaction problem can be decomposed into two parts. One is an infinite domain with circular boundaries. The other is an interior problem for each cylinder. The interface condition for the porous cylinder is considered as a similar idea of complex spring in the structural dynamics. Force as well as free-surface elevation were calculated and compared with others to check the validity of our formulation. The parameter study for the disorder and porosity on the effect of near-trapped modes will be investigated.

2、 Problem statement and integral formulation

2.1 Problem statement

Irrotational motion of the inviscid and incompressible fluid is small-amplitude which is defined as velocity potential $\Phi(x,y,z,t)$ based on the linear water wave theory. We assume that there are *N* vertical circular cylinders mounted at $z=-h$ upward to the free surface as shown in Fig. 1. The governing equation of the water wave problem is the Laplace equation

$$\nabla^2\Phi(x,y,z,t)=0,\ (x,y,z)\in D. \qquad (1)$$

where ∇^2 and *D* are the Laplacian operator and the domain of interest, respectively. For satisfying the boundary conditions of seabed, kinematic boundary conditions and dynamic boundary condition at free surface as shown below:

$$-\frac{\partial \Phi}{\partial n}=0,\quad z=-h(x,y), \tag{2}$$

$$-\Phi_z=\varphi_t-\Phi_x\varphi_x-\Phi_y\varphi_y,\quad z=\varphi(x,y,t), \tag{3}$$

$$-\Phi_t+gz+\frac{1}{2}(\Phi_x^2+\Phi_y^2+\Phi_z^2),\quad z=\varphi(x,y,t), \tag{4}$$

where g is the acceleration of gravity and $\varphi(x,y,t)$ is the free-surface elevation, we assume

$$\Phi(x,y,z,t)=\mathrm{Re}\{u(x,y)f(z)e^{-i\omega t}\}, \tag{5}$$

where

$$f(z)=\frac{-igA}{\omega}\frac{\cosh k(z+h)}{\cosh kh}, \tag{6}$$

in which A is the amplitude of incident wave, ω denotes the angular frequency, k represents the wave number, and $\boldsymbol{i}^2=-1$ The free-surface elevation is defined by

$$\varphi(x,y,t)=\mathrm{Re}\{\eta(x,y)e^{-i\omega t}\}, \tag{7}$$

where

$$\eta(x,y)=Au(x,y). \tag{8}$$

The potential of incident wave $u_{inc}(x,y)$ is shown below:

$$u_{inc}(x,y)=e^{ik(x\cos\theta_{inc}+y\sin\theta_{inc})}\equiv e^{ik\rho\cos(\phi-\theta_{inc})}, \tag{9}$$

where θ_{inc} is the angle of incident wave, $\rho=\sqrt{x^2+y^2}$ and $\phi=\arctan(y/x)$. Substituting Eq. (5) into Eq. (1), we have

$$(\nabla^2+k^2)u(x,y)=0,\ (x,y)\in D. \tag{10}$$

The boundary conditions are shown below:

$$\frac{\partial u^O}{\partial r}=-\frac{\partial u_j^C}{\partial r}=ikG\left(u_j^C-u^O\right), \tag{11}$$

where the superscripts "*O*" and "*C*" denote the regions of ocean and cylinder, respectively, G is the dimensionless parameter of porosity and the dispersion relationship is

$$k\tanh kh=\frac{\omega^2}{g}. \tag{12}$$

The dynamic pressure can be obtained by

$$\begin{aligned} p&=-\rho_f\frac{\partial\Phi}{\partial t}\\ &=-\rho_f gA\frac{\cosh k(z+h)}{\cosh kh}u(x,y)e^{-i\omega t}, \end{aligned} \tag{13}$$

where ρ_f is the density of the fluid. The two components of the first-order force X^j on the *j*th cylinder are given by integrating the pressure over the circular boundary as shown below:

$$\begin{aligned} X^j&=-\frac{\rho_f gAa_j}{k}\tanh kh\\ &\int_0^{2\pi}u(x,y)\begin{Bmatrix}\cos\theta_j\\ \sin\theta_j\end{Bmatrix}d\theta_j, \end{aligned} \tag{14}$$

where a_j denotes the radius of the *j*th cylinder.

2.2 Dual integral equations — the conventional version

The boundary integral equation for the domain point can be derived from the Green's third identity [19], we have

$$\begin{aligned} 2\pi u(\boldsymbol{x})&=\int_B T(s,x)u(s)dB(s)\\ &\quad-\int_B U(s,x)t(s)dB(s),\ x\in D, \end{aligned} \tag{15}$$

$$\begin{aligned} 2\pi t(\boldsymbol{x})&=\int_B M(s,x)u(s)dB(s)\\ &\quad-\int_B L(s,x)t(s)dB(s),\ x\in D, \end{aligned} \tag{16}$$

where s and x are the source and field points, respectively, $t(s)=\dfrac{\partial u(s)}{\partial n_s}$, B is the boundary, n_s and n_x denote the outward normal vectors at the source point *s* and field point *x*, respectively. The kernel function $U(\mathbf{s},\mathbf{x})$ is the fundamental solution which satisfies

$$\nabla^2U(\mathbf{s},\mathbf{x})=2\pi\delta(\mathbf{x}-\mathbf{s}) \tag{17}$$

in which $\delta(\mathbf{x}-\mathbf{s})$ denotes the Dirac-delta function. Then, we can obtain the fundamental solution as follows:

$$U(\mathbf{s},\mathbf{x})=\frac{-i\pi H_0^{(1)}\left(kr\right)}{2} \tag{18}$$

where $H_0^{(1)}(kr)$ is the zeroth Hankel function of the first kind and $r\equiv|s-x|$. The other kernels functions, $T(\mathbf{s},\mathbf{x})$, $L(\mathbf{s},\mathbf{x})$, and $M(\mathbf{s},\mathbf{x})$, are defined by

$$T(\mathbf{s},\mathbf{x})=\frac{\partial U(\mathbf{s},\mathbf{x})}{\partial n_s}, \tag{19}$$

$$L(\mathbf{s},\mathbf{x})=\frac{\partial U(\mathbf{s},\mathbf{x})}{\partial n_x}, \tag{20}$$

$$M(\mathbf{s},\mathbf{x})=\frac{\partial^2U(\mathbf{s},\mathbf{x})}{\partial n_s\partial n_x}. \tag{21}$$

By moving the field point *x* to the boundary, the dual boundary integral equations for the boundary point can be obtained as follows:

$$\begin{aligned} \pi u(\mathbf{x})&=C.P.V.\int_B T(\mathbf{s},\mathbf{x})u(\mathbf{s})dB(\mathbf{s})\\ &\quad-R.P.V.\int_B U(\mathbf{s},\mathbf{x})t(\mathbf{s})dB(\mathbf{s}),\ x\in B, \end{aligned} \tag{22}$$

$$\begin{aligned} \pi t(\mathbf{x})&=H.P.V.\int_B M(\mathbf{s},\mathbf{x})u(\mathbf{s})dB(\mathbf{s})\\ &\quad-C.P.V.\int_B L(\mathbf{s},\mathbf{x})t(\mathbf{s})dB(\mathbf{s}),\ x\in B, \end{aligned} \tag{23}$$

where *R.P.V.*, *C.P.V.* and *H.P.V.* denote the Riemann principal value, Cauchy principal value and Hadamard (or called Mangler) principal value, respectively. By pushing the field point to the complementary domain, the dual null-field integral equations are given below:

$$0=\int_B T(\mathbf{s},\mathbf{x})u(\mathbf{s})dB(\mathbf{s}) - \int_B U(\mathbf{s},\mathbf{x})t(\mathbf{s})dB(\mathbf{s}),\ x\in D^c, \tag{24}$$

$$0=\int_B M(\mathbf{s},\mathbf{x})u(\mathbf{s})dB(\mathbf{s}) - \int_B L(\mathbf{s},\mathbf{x})t(\mathbf{s})dB(\mathbf{s}),\ x\in D^c, \tag{25}$$

where D^c is the complementary domain. Eqs. (15), (16), (24) and (25) are conventional formulations where the point can not be located on the real boundary. Singularity occurs and concept of principal values are required once Eqs. (22) and (23) are considered.

2.3 Dual boundary integral formulation — the present version

By introducing the degenerate kernel, the collocation point can be exactly located on the real boundary free of calculating singular integrals in the sense of principal value. Therefore, the integral equations for the domain point and null-field integral equations in the interior problem are represented as

$$2\pi u(\mathbf{x})=\int_B T^I(\mathbf{s},\mathbf{x})u(\mathbf{s})dB(\mathbf{s}) - \int_B U^I(\mathbf{s},\mathbf{x})t(\mathbf{s})dB(\mathbf{s}),\ x\in D\cup B, \tag{26}$$

$$2\pi t(\mathbf{x})=\int_B M^I(\mathbf{s},\mathbf{x})u(\mathbf{s})dB(\mathbf{s}) - \int_B L^I(\mathbf{s},\mathbf{x})t(\mathbf{s})dB(\mathbf{s}),\ x\in D\cup B, \tag{27}$$

and

$$0=\int_B T^E(\mathbf{s},\mathbf{x})u(\mathbf{s})dB(\mathbf{s}) - \int_B U^E(\mathbf{s},\mathbf{x})t(\mathbf{s})dB(\mathbf{s}),\ x\in D^c\cup B, \tag{28}$$

$$0=\int_B M^E(\mathbf{s},\mathbf{x})u(\mathbf{s})dB(\mathbf{s}) - \int_B L^E(\mathbf{s},\mathbf{x})t(\mathbf{s})dB(\mathbf{s}),\ x\in D^c\cup B. \tag{29}$$

For the exterior problem, the domain of interest is in the external region of the circular boundary and the complementary domain is in the internal region of the circle. Therefore, the null-field integral equations are represented as

$$2\pi u(\mathbf{x})=\int_B T^E(\mathbf{s},\mathbf{x})u(\mathbf{s})dB(\mathbf{s}) - \int_B U^E(\mathbf{s},\mathbf{x})t(\mathbf{s})dB(\mathbf{s}),\ x\in D\cup B, \tag{30}$$

$$2\pi t(\mathbf{x})=\int_B M^E(\mathbf{s},\mathbf{x})u(\mathbf{s})dB(\mathbf{s}) - \int_B L^E(\mathbf{s},\mathbf{x})t(\mathbf{s})dB(\mathbf{s}),\ x\in D\cup B, \tag{31}$$

and

$$0=\int_B T^I(\mathbf{s},\mathbf{x})u(\mathbf{s})dB(\mathbf{s}) - \int_B U^I(\mathbf{s},\mathbf{x})t(\mathbf{s})dB(\mathbf{s}),\ x\in D^c\cup B, \tag{32}$$

$$0=\int_B M^I(\mathbf{s},\mathbf{x})u(\mathbf{s})dB(\mathbf{s}) - \int_B L^I(\mathbf{s},\mathbf{x})t(\mathbf{s})dB(\mathbf{s}),\ x\in D^c\cup B, \tag{33}$$

where the superscripts of "*I*" and "*E*" denote interior and exterior degenerate kernels for fundamental solutions. The explicit forms of degenerate kernels will be elaborated on later.

2.4 Expansions of fundamental solution and boundary density

Based on the separable property, the kernel function $U(\mathbf{s},\mathbf{x})$ can be expanded into degenerate form by separating the source point and field point in the polar coordinates. Since degenerate kernels can describe the fundamental solutions in two regions (interior and exterior domains), the BIE for the domain point in Eqs. (26)-(27) and Eqs. (30)-(31) and the null-field BIE in Eqs. (28)-(29) and Eqs. (32)-(33), can be directly employed for the real boundary point. By using the polar coordinates, we can express $\mathbf{x}=(\rho,\phi)$ and $\mathbf{s}=(R,\theta)$. The four kernels *U, T, L* and *M* can be expressed in terms of degenerate kernels [20] as shown below:

$$U(\mathbf{s},\mathbf{x})=\begin{cases} U^I(R,\theta;\rho,\phi)=\dfrac{-\pi i}{2}\sum_{m=0}^{\infty}\varepsilon_m J_m(k\rho) H_m^{(1)}(kR)\cos(m(\theta-\phi)), & R\ge\rho, \\ U^E(R,\theta;\rho,\phi)=\dfrac{-\pi i}{2}\sum_{m=0}^{\infty}\varepsilon_m H_m^{(1)}(k\rho) J_m(kR)\cos(m(\theta-\phi)), & R<\rho, \end{cases} \tag{34}$$

$$T(\mathbf{s},\mathbf{x})=\begin{cases} T^I(R,\theta;\rho,\phi)=\dfrac{-\pi ki}{2}\sum_{m=0}^{\infty}\varepsilon_m J_m(k\rho) H_m'^{(1)}(kR)\cos(m(\theta-\phi)), & R>\rho, \\ T^E(R,\theta;\rho,\phi)=\dfrac{-\pi ki}{2}\sum_{m=0}^{\infty}\varepsilon_m H_m^{(1)}(k\rho) J_m'(kR)\cos(m(\theta-\phi)), & R<\rho, \end{cases} \tag{35}$$

$$L(\mathbf{s},\mathbf{x})=\begin{cases} L^I(R,\theta;\rho,\phi)=\dfrac{-\pi ki}{2}\sum_{m=0}^{\infty}\varepsilon_m J_m'(k\rho) H_m^{(1)}(kR)\cos(m(\theta-\phi)), & R>\rho, \\ L^E(R,\theta;\rho,\phi)=\dfrac{-\pi ki}{2}\sum_{m=0}^{\infty}\varepsilon_m H_m'^{(1)}(k\rho) J_m(kR)\cos(m(\theta-\phi)), & R<\rho, \end{cases} \tag{36}$$

$$M(\mathbf{s},\mathbf{x})=\begin{cases} M^I(R,\theta;\rho,\phi)=\dfrac{-\pi k^2 i}{2}\sum_{m=0}^{\infty}\varepsilon_m J_m'(k\rho) H_m'^{(1)}(kR)\cos(m(\theta-\phi)), & R\ge\rho, \\ M^E(R,\theta;\rho,\phi)=\dfrac{-\pi k^2 i}{2}\sum_{m=0}^{\infty}\varepsilon_m H_m'^{(1)}(k\rho) J_m'(kR)\cos(m(\theta-\phi)), & R<\rho, \end{cases} \tag{37}$$

where ε_m is the Neumann factor

$$\varepsilon_m = \begin{cases} 1, & m = 0, \\ 2, & m = 1,\ 2,\ \cdots, \infty. \end{cases} \tag{38}$$

Mathematically speaking, the expressions of fundamental solutions in Eqs. (34)-(37) are termed degenerate kernels (or separable kernels) which can expand the kernel to sums of products of function of the field point *x* alone and function of the source point **s** alone. If the finite sum of series is considered, the kernel is finite rank. As we shall see in the later sections, the theory of boundary integral equations with degenerate kernel is nothing more than the linear algebra. Since the potentials resulted from $T(\mathbf{s},\mathbf{x})$ and $L(\mathbf{s},\mathbf{x})$ are discontinuous across the boundary, the equal sign between ρ and R is not included in the expression for the degenerate kernels of $T(\mathbf{s},\mathbf{x})$ and $L(\mathbf{s},\mathbf{x})$ in Eqs. (35) and (36).

The degenerate kernels simply serve as the means to evaluate regular integrals analytically and take the limit to boundary analytically. The reason is that integral equation for the domain point of Eq. (26) and the null-field integral equation of Eq. (28) yield the same algebraic equation when the limit is taken from the inside or from the outside of the region. Both limits represent the same algebraic equation that is an approximate counterpart of the boundary integral equation, that for the case of a smooth boundary has in the left-hand side term $\pi u(\mathbf{x})$ or $\pi t(\mathbf{x})$ rather than $2\pi u(\mathbf{x})$ or $2\pi t(\mathbf{x})$ for the domain point or 0 for the point outside the domain. Besides, the limiting case to the boundary is also addressed. The continuous and jump behavior across the boundary is well captured by the Wronskian property of Bessel function J_m and Y_m bases

$$W(J_m(kR), Y_m(kR)) = Y_m'(kR)J_m(kR) - Y_m(kR)J_m'(kR) = \frac{2}{\pi kR} \tag{39}$$

as shown below

$$\int_0^{2\pi} \left(T^I(\mathbf{s},\mathbf{x}) - T^E(\mathbf{s},\mathbf{x})\right)\cos(m\theta)Rd\theta = 2\pi\cos(m\phi),\ x \in B, \tag{40}$$

$$\int_0^{2\pi} \left(T^I(\mathbf{s},\mathbf{x}) - T^E(\mathbf{s},\mathbf{x})\right)\sin(m\theta)Rd\theta = 2\pi\sin(m\phi),\ x \in B. \tag{41}$$

After employing Eqs. (40)-(41), Eq.(30) and Eq. (32) yield the same linear algebraic equation when *x* is exactly located the boundary from the domain or the complementary domain. A proof for the Laplace case can be found by [21].

In order to fully utilize the geometry of circular boundary, the boundary potential $u(\mathbf{s})$ and its normal flux $t(\mathbf{s})$ can be approximated by employing the Fourier series. Therefore, we assume

$$u(\mathbf{s}) = a_0 + \sum_{n=1}^{\infty}(a_n\cos n\theta + b_n\sin n\theta), \tag{42}$$

$$t(\mathbf{s}) = p_0 + \sum_{n=1}^{\infty}(p_n\cos n\theta + q_n\sin n\theta), \tag{43}$$

where a_0, a_n, b_n, p_0, p_n and q_n are the Fourier coefficients Eqs. (32) and (33) can be easily calculated by employing the orthogonal property of Fourier series. In the real computation, only the finite *M* terms are used in the summation of Eqs. (42) and (43).

2.5 Adaptive observer system

Since the boundary integral equations are frame indifferent, *i.e.* rule of objectivity is obeyed. Adaptive observer system is chosen to fully employ the property of degenerate kernels. Fig. 2 shows the boundary integration for the circular boundaries. It is worthy of noting that the origin of the observer system can be adaptively located on the center of the corresponding circle under integration to fully utilize the geometry of circular boundary. The dummy variable in the integration on the circular boundary is just the angle (θ) instead of the radial coordinate (R). By using the adaptive observer system, all the boundary integrals can be determined analytically free of principal value.

2.6 Linear algebraic equation

After locating the null-field point $\mathbf{x}_k$ exactly on the *k*th circular boundary in Eq. (28) as shown in Fig. 2, we have

$$0 = \sum_{k=0}^{N}\int_{B_k} T^E(\mathbf{s},\mathbf{x})u(\mathbf{s})dB(\mathbf{s}) - \sum_{k=0}^{N}\int_{B_k} U^E(\mathbf{s},\mathbf{x})t(\mathbf{s})dB(\mathbf{s}),\ x \in D^c \cup B, \tag{44}$$

where *N* is the number of circular cylinders and B_0 denotes the outer boundary for the bounded domain. In case of the infinite problem in Fig. 3(a), B_0 becomes a circular boundary with an infinite radius. If the radiation condition at infinity is satisfied, the B_0 integration is null. The origin of observer system is adaptively chosen at the center of circular boundary under integration. The dummy variable in the circular integration is angle (θ) instead of radial coordinate (R). In the real computation, we select the collocation point on the boundary and the integration path is counterclockwise for the outer circle. Otherwise, it is clockwise. For the integration path B_k, the kernels of $U(\mathbf{s},\mathbf{x})$ and $T(\mathbf{s},\mathbf{x})$ are respectively expressed in terms of degenerate kernels of Eqs. (34) and (35) with respect to the observer origin at the center of the corresponding path. The boundary densities of $u(\mathbf{s})$ and $t(\mathbf{s})$ are substituted by using the Fourier series of Eqs. (42)

and (43), respectively. In the B_k integration, we set the origin of the observer system to collocate at the center c_k of B_k to fully utilize the degenerate kernel and Fourier series. By moving the null-field point exactly on the real boundary B_k from outside of the domain D^c in the numerical implementation, a linear algebraic system is obtained. For the exterior problem of infinite domain in Fig. 3(b), we have

$$[\mathbf{U}^I]\{\mathbf{t}^O-\mathbf{t}^{inc}\}=[\mathbf{T}^I]\{\boldsymbol{u}^O-\boldsymbol{u}^{inc}\} \tag{45}$$

For the interior problem of each cylinder in Fig. 3(c), we have

$$[\mathbf{U}^E]\{\mathbf{t}^C\}=[\mathbf{T}^E]\{\boldsymbol{u}^C\} \tag{46}$$

$[\mathbf{U}^I]$, $[\mathbf{T}^I]$, $[\mathbf{U}^E]$ and $[\mathbf{T}^E]$ are the influence matrices with a dimension of $N\times(2M+1)$ by $N\times(2M+1)$, $\{\mathbf{t}^O\}$, $\{\mathbf{t}^{inc}\}$, $\{\boldsymbol{u}^O\}$, $\{\boldsymbol{u}^{inc}\}$, $\{\mathbf{t}^C\}$ and $\{\mathbf{u}^C\}$ denote the column vectors of Fourier coefficients with a dimension of $N\times(2M+1)$ by 1 in which those are defined as follows:

$$[\mathbf{U}^I]=\begin{bmatrix}\mathbf{U}^I_{00} & \mathbf{U}^I_{01} & \cdots & \mathbf{U}^I_{0N}\\ \mathbf{U}^I_{10} & \mathbf{U}^I_{11} & \cdots & \mathbf{U}^I_{1N}\\ \vdots & \vdots & \ddots & \vdots\\ \mathbf{U}^I_{N0} & \mathbf{U}^I_{N1} & \cdots & \mathbf{U}^I_{NN}\end{bmatrix}, \tag{47}$$

$$[\mathbf{T}^I]=\begin{bmatrix}\mathbf{T}^I_{00} & \mathbf{T}^I_{01} & \cdots & \mathbf{T}^I_{0N}\\ \mathbf{T}^I_{10} & \mathbf{T}^I_{11} & \cdots & \mathbf{T}^I_{1N}\\ \vdots & \vdots & \ddots & \vdots\\ \mathbf{T}^I_{N0} & \mathbf{T}^I_{N1} & \cdots & \mathbf{T}^I_{NN}\end{bmatrix}, \tag{48}$$

$$[\mathbf{U}^E]=\begin{bmatrix}\mathbf{U}^E_{00} & 0 & \cdots & 0\\ 0 & \mathbf{U}^E_{11} & \cdots & 0\\ \vdots & \vdots & \ddots & \vdots\\ 0 & 0 & \cdots & \mathbf{U}^E_{NN}\end{bmatrix}, \tag{49}$$

$$[\mathbf{T}^E]=\begin{bmatrix}\mathbf{T}^E_{00} & 0 & \cdots & 0\\ 0 & \mathbf{T}^E_{11} & \cdots & 0\\ \vdots & \vdots & \ddots & \vdots\\ 0 & 0 & \cdots & \mathbf{T}^E_{NN}\end{bmatrix}, \tag{50}$$

$$\{\boldsymbol{u}^O\}=\begin{Bmatrix}\boldsymbol{u}^O_0\\ \boldsymbol{u}^O_1\\ \vdots\\ \boldsymbol{u}^O_N\end{Bmatrix},\ \{\boldsymbol{u}^{inc}\}=\begin{Bmatrix}\boldsymbol{u}^{inc}_0\\ \boldsymbol{u}^{inc}_1\\ \vdots\\ \boldsymbol{u}^{inc}_N\end{Bmatrix},$$

$$\{\mathbf{t}^O\}=\begin{Bmatrix}\mathbf{t}^O_0\\ \mathbf{t}^O_1\\ \vdots\\ \mathbf{t}^O_N\end{Bmatrix},\ \{\mathbf{t}^{inc}\}=\begin{Bmatrix}\mathbf{t}^{inc}_0\\ \mathbf{t}^{inc}_1\\ \vdots\\ \mathbf{t}^{inc}_N\end{Bmatrix}, \tag{51}$$

$$\{\boldsymbol{u}^C\}=\begin{Bmatrix}\boldsymbol{u}^C_0\\ \boldsymbol{u}^C_1\\ \vdots\\ \boldsymbol{u}^C_N\end{Bmatrix},\ \{\mathbf{t}^C\}=\begin{Bmatrix}\mathbf{t}^C_0\\ \mathbf{t}^C_1\\ \vdots\\ \mathbf{t}^C_N\end{Bmatrix}, \tag{52}$$

the first subscript " j " (j =1, 2, …, N) in $[\mathbf{U}^E]$, $[\mathbf{T}^E]$, $[\mathbf{U}^I]$ and $[\mathbf{T}^I]$ denotes the index of the jth circular boundary where the collocation point is located and the second subscript " k " (k =1, 2, …, N) denotes the index of the *kth* circular boundary when integrating on each boundary data $\{\mathbf{t}^O-\mathbf{t}^{inc}\}$, $\{\boldsymbol{u}^O-\boldsymbol{u}^{inc}\}$ in Fig. 3(d), $\{\mathbf{t}^C\}$ and $\{\boldsymbol{u}^C\}$ in Fig. 3(c), N is the number of circular cylinders in the domain and the number M indicates the truncated terms of Fourier series. It is noted that $\{\boldsymbol{u}^{inc}\}$ and $\{\boldsymbol{t}^{inc}\}$ in Fig. 3(e) are the free-surface elevation and flux due to the incident wave. The coefficient matrix of the linear algebraic system is partitioned into blocks, and each off-diagonal block corresponds to the influence matrices between two different circular boundaries. The diagonal blocks are the influence matrices due to itself in each individual circle. After uniformly collocating the point along the kth circular boundary, the submatrix can be written as

$$[\mathbf{U}_{jk}]=\begin{bmatrix}\mathbf{U}^{0c}_{jk}(\phi_1) & \mathbf{U}^{1c}_{jk}(\phi_1) & \mathbf{U}^{2s}_{jk}(\phi_1) & \cdots & \mathbf{U}^{Mc}_{jk}(\phi_1) & \mathbf{U}^{Ms}_{jk}(\phi_1)\\ \mathbf{U}^{0c}_{jk}(\phi_2) & \mathbf{U}^{1c}_{jk}(\phi_2) & \mathbf{U}^{2s}_{jk}(\phi_2) & \cdots & \mathbf{U}^{Mc}_{jk}(\phi_2) & \mathbf{U}^{Ms}_{jk}(\phi_2)\\ \mathbf{U}^{0c}_{jk}(\phi_3) & \mathbf{U}^{1c}_{jk}(\phi_3) & \mathbf{U}^{2s}_{jk}(\phi_3) & \cdots & \mathbf{U}^{Mc}_{jk}(\phi_3) & \mathbf{U}^{Ms}_{jk}(\phi_3)\\ \vdots & \vdots & \vdots & \ddots & \vdots & \vdots\\ \mathbf{U}^{0c}_{jk}(\phi_{2M}) & \mathbf{U}^{1c}_{jk}(\phi_{2M}) & \mathbf{U}^{2s}_{jk}(\phi_{2M}) & \cdots & \mathbf{U}^{Mc}_{jk}(\phi_{2M}) & \mathbf{U}^{Ms}_{jk}(\phi_{2M})\\ \mathbf{U}^{0c}_{jk}(\phi_{2M+1}) & \mathbf{U}^{1c}_{jk}(\phi_{2M+1}) & \mathbf{U}^{2s}_{jk}(\phi_{2M+1}) & \cdots & \mathbf{U}^{Mc}_{jk}(\phi_{2M+1}) & \mathbf{U}^{Ms}_{jk}(\phi_{2M+1})\end{bmatrix} \tag{53}$$

$$[\mathbf{T}_{jk}]=\begin{bmatrix} \mathbf{T}_{jk}^{0c}(\phi_1) & \mathbf{T}_{jk}^{1c}(\phi_1) & \mathbf{T}_{jk}^{2s}(\phi_1) & \cdots & \mathbf{T}_{jk}^{Mc}(\phi_1) & \mathbf{T}_{jk}^{Ms}(\phi_1) \\ \mathbf{T}_{jk}^{0c}(\phi_2) & \mathbf{T}_{jk}^{1c}(\phi_2) & \mathbf{T}_{jk}^{2s}(\phi_2) & \cdots & \mathbf{T}_{jk}^{Mc}(\phi_2) & \mathbf{T}_{jk}^{Ms}(\phi_2) \\ \mathbf{T}_{jk}^{0c}(\phi_3) & \mathbf{T}_{jk}^{1c}(\phi_3) & \mathbf{T}_{jk}^{2s}(\phi_3) & \cdots & \mathbf{T}_{jk}^{Mc}(\phi_3) & \mathbf{T}_{jk}^{Ms}(\phi_3) \\ \vdots & \vdots & \vdots & \ddots & \vdots & \vdots \\ \mathbf{T}_{jk}^{0c}(\phi_{2M}) & \mathbf{T}_{jk}^{1c}(\phi_{2M}) & \mathbf{T}_{jk}^{2s}(\phi_{2M}) & \cdots & \mathbf{T}_{jk}^{Mc}(\phi_{2M}) & \mathbf{T}_{jk}^{Ms}(\phi_{2M}) \\ \mathbf{T}_{jk}^{0c}(\phi_{2M+1}) & \mathbf{T}_{jk}^{1c}(\phi_{2M+1}) & \mathbf{T}_{jk}^{2s}(\phi_{2M+1}) & \cdots & \mathbf{T}_{jk}^{Mc}(\phi_{2M+1}) & \mathbf{T}_{jk}^{Ms}(\phi_{2M+1}) \end{bmatrix} \tag{54}$$

where ϕ_k ($k=1,\ 2,\ \cdots,\ 2M+1$) is the polar angle of the collocating point $\boldsymbol{x}_m$ along the boundary. It is noted that the superscript "0s" in Eq. (53) disappears since $\sin(0\theta)=0$, and the element of $[\mathbf{U}_{jk}]$ and $[\mathbf{T}_{jk}]$ are defined as-

$$U_{jk}^{nc}=\int_{B_k}U(\mathbf{s}_k,\mathbf{x}_m)\cos(n\theta_k)R_k d\theta_k \tag{55}$$

$$U_{jk}^{ns}=\int_{B_k}U(\mathbf{s}_k,\mathbf{x}_m)\sin(n\theta_k)R_k d\theta_k \tag{56}$$

$$T_{jk}^{nc}=\int_{B_k}T(\mathbf{s}_k,\mathbf{x}_m)\cos(n\theta_k)R_k d\theta_k \tag{57}$$

$$T_{jk}^{ns}=\int_{B_k}T(\mathbf{s}_k,\mathbf{x}_m)\sin(n\theta_k)R_k d\theta_k \tag{58}$$

where $n=1,\ 2,\ \cdots,\ M$. By matching interface condition of in Eq. (11) and assembling matrices of Eqs. (45) and (46), we have

$$\begin{bmatrix} \boldsymbol{T}^{\boldsymbol{I}} & -\boldsymbol{U}^{\boldsymbol{I}} & 0 & 0 \\ 0 & 0 & \boldsymbol{T}^{\boldsymbol{E}} & -\boldsymbol{U}^{\boldsymbol{E}} \\ 0 & -\boldsymbol{I} & 0 & -\boldsymbol{I} \\ \boldsymbol{ikG} & 0 & -\boldsymbol{ikG} & \boldsymbol{I} \end{bmatrix} \begin{Bmatrix} \boldsymbol{u}^{\boldsymbol{O}} \\ \boldsymbol{t}^{\boldsymbol{O}} \\ \boldsymbol{u}^{\boldsymbol{C}} \\ \boldsymbol{t}^{\boldsymbol{C}} \end{Bmatrix} = \begin{bmatrix} \boldsymbol{W}_{\boldsymbol{inc}} \\ 0 \\ 0 \\ 0 \end{bmatrix}, \tag{59}$$

where the matrix $[I]$ is an identity matrix and $\boldsymbol{W}_{\boldsymbol{inc}}=\left[\boldsymbol{T}^{\boldsymbol{I}}\right]\left\{\boldsymbol{u}^{\boldsymbol{inc}}\right\}-\left[\boldsymbol{U}^{\boldsymbol{I}}\right]\left\{\boldsymbol{t}^{\boldsymbol{inc}}\right\}$ is the forcing term. After obtaining the unknown Fourier coefficients, we can obtain the free-surface elevation by using Eq. (30).

2.7 Perturbation of ordered cylinder arrangements

An arrangement of 16 cylinders according to a regular three-rows disposition is shown in Fig. 5. For the purpose of disturbing the regular arrangement, a perturbation of disposition is given. The displacement of each cylinder center apart from its original periodical position is defined as follows:

$$\begin{aligned} \Delta x_j &= \gamma_j p\tau\cos\left(2\pi\gamma_j\right), \\ \Delta y_j &= \gamma_j p\tau\sin\left(2\pi\gamma_j\right), \end{aligned} \tag{60}$$

where γ_j is a random variable in the range [0,1], the maximum permissible displacement p is equal to d-a and τ is a global disorder parameter. The distance between the two centers of identical cylinders is 2d where the radii of cylinders are a.

3、 Illustrative examples

Configuration of five sets of sixteen cylinders is depicted in Fig. 5. Contour plots of the maximum free-surface elevation are shown in Figs. 6(a) and (b) by using the Duclos and Clèment's method [17] and our approach, respectively. A trapped mode appears at the wave number of k=4.08482.

Effect of disorder

As shown in Fig. 6(a), original state without disorder and porous effect is considered. Here, the effect of disorder is our main concern. Following the definition of disorder parameter $\boldsymbol{\tau}$, two random cases of $\boldsymbol{\tau}=0.1$ were reported by Duclos and Clèment [17] as shown in Figs. 7(a) and (b). The appearance of the trapped mode is dramatically suppressed. To test the accuracy of our approach for the disorder effect, Fig. 8 shows that the contour plots of the trapped modes are effectively suppressed for $\boldsymbol{\tau}=0.1$, respectively.

Effect of porosity

To verify the effect of porous parameter on the trapped mode of sixteen cylinders in Fig. 6, Fig. 9 shows the contour of the maximum free-surface elevation. The maximum value of 150 reduces to 75 due to the porous parameter of G=1.0.

Effect of porous parameter and disorder together

To verify both the effects of disorder and porosity, a sixteen-cylinders example is demonstrated here. Figure 6 shows the contour of the free-surface elevation without disorder and porosity. By considering the perturbation parameter $\tau=0.1$, the maximum free-surface elevation dramatically reduces to 3.90 from the original value of 150 in Fig. 8. By only considering the porous cylinder without disorder, the maximum free-surface elevation in Fig. 7 is reduced to half (75) in Fig. 6 (150). If the perturbation parameter and porosity are simultaneously considered, the maximum free-surface elevation reduces to 2.70 in Fig. 9. It indicates that disorder dominate the maximum free-surface elevation.

4、 Conclusions

In this paper, not only a systematic approach was employed to investigate the water-wave interaction with arrays of surface-piercing porous cylinders, but also the effect of porosity and disorder on the force in case of trapped modes was also examined. The case of impermeable cylinder case can be treated as a special case with G=0. Addition theorem or so-called the degenerate kernel is adopted in the null-field integral formulation. Therefore, the singular integrals using bump integrals for principal values can be avoided. Numerical results including the free-surface elevation and resultant forces on each cylinder have been presented to illustrate the effect of porous and disorder parameters on the force in case of trapped modes. It is found that the disorder is more sensitive to suppress the occurrence of near-trapped modes than the porosity. Good agreements are observed after comparing with the results obtained in the literature.

References

[1] MacCamy, R. C., and Fuchs, R. A., "Wave force on piles: A diffraction theory", Technical Memorandum No. 69 U. S. Army Coastal Engineering Research Center (formerly Beach Erosion Board), 1954.

[2] Spring, B. H., and Monkmeyer, P. L., "Interaction of plane waves with vertical cylinders", Proceeding 14th International Conference on Coastal Engineering, pp 1828-1845, 1974.

[3] Linton, C. M., and Evans, D. V., "The interaction of waves with arrays of vertical circular cylinders", Journal of Fluid Mechanics, Vol 215, pp 549-569, 1990.

[4] Morse, P. M., Feshbach, H., "Methods of theoretical physics", New York: McGraw-Hill, 1978.

[5] Martin, P. A., "Multiple Scattering. Interaction of time-harmonic waves with N obstacles", New York: Cambridge University Press, 2006.

[6] Chatjigeorgiou, I. K., Mavrakos, S. A., "Hydrodynamic diffraction by multiple elliptical cylinders", The 24th International Workshop on Water Waves and Floating Bodies, Zelenogorsk, Russia, 2009.

[7] Au, M. C., and Brebbia, C. A., "Numerical prediction of wave forces using the boundary element method", Applied Mathematical Modelling , Vol 6, pp 218-228, 1982.

[8] Au, M. C., and Brebbia, C. A., "Diffraction of water waves for vertical cylinders using boundary elements", Applied Mathematical Modelling, Vol 7, pp 106-114, 1983.

[9] Zhu, S. P., and Moule, G., "An Efficient Numerical Calculation of Wave Loads on an Array of Vertical Cylinders", Applied Mathematical Modelling, Vol 20, pp 26-33, 1996.

[10] Chen Y. H., "Wave-induced oscillations in harbors by permeable arc breakwaters", Master Thesis, National Taiwan Ocean University, Keelung, 2004.

[11] Chen, J. T., Lee, Y. T. and Lin, Y. J., "Interaction of water waves with arbitrary vertical cylinders using null-field integral equations", Applied Ocean Research, Accepted, 2009.

[12] Evans, D. V., and Porter, R., "Trapped modes about multiple cylinders in a channel", Journal of Fluid Mechanics, Vol 339, pp 331-356, 1997.

[13] Maniar, H. D., and Newman, J. N., "Wave diffraction by a long array of cylinders", Journal of Fluid Mechanics, Vol 339, pp309-330, 1997.

[14] Evans, D. V., and Porter, R., "Trapping and near-trapping by arrays of cylinders in waves", Journal of Fluid Mechanics, Vol 35, pp 149-179, 1999.

[15] Thompson, I., Linton, C. M., and Porter, R., "A new approximation method for scattering by long finite arrays", The Quarterly Journal of Mechanics and Applied Mathematics, Vol 25, pp 333-352, 2008.

[16] Linton, C. M., and McIver, P., "Embedded trapped modes in water waves and acoustics", Wave Motion, Vol 45, pp 16-29, 2007.

[17] Duclos, G., and Clèment, A. H., "Wave propagation through arrays of unevenly spaced vertical piles", Ocean Engineering, Vol 31, pp 1655-1668, 2004.

[18] Williams, A. N., and Li, W., "Water wave interaction with an array of bottom-mounted surface-piercing porous cylinders", Ocean Engineering, Vol 27, pp 841-866, 2000.

[19] Chen, J. T., Chen, K. H., Chen, I. L. and Liu, L. W., "A new concept of modal participation factor for numerical instability in the dual BEM for exterior acoustics", Mechanics Research Communications, Vol 26, No 2, pp 161-174, 2003.

[20] Chen, J. T., Chen, C. T., Chen, P. Y., Chen, I. L., "A semi-analytical approach for radiation and scattering", Computer Methods in Applied Mechanics and Engineering, Vol 196, pp 2751-2764, 2007.

[21] Chen, J. T., Shen, W. C., and Wu, A. C., "Null-field integral equations for stress field around circular holes under antiplane shear", Engineering Analysis with Boundary Elements, Vol 30, pp 205-217, 2006.

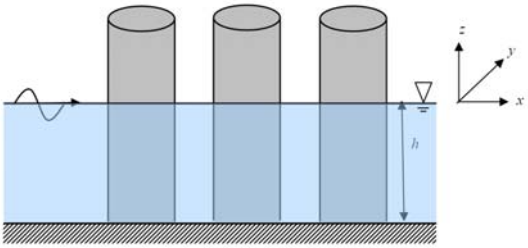

Figure 1 Problem statement of water waves with an array of vertical cylinders.

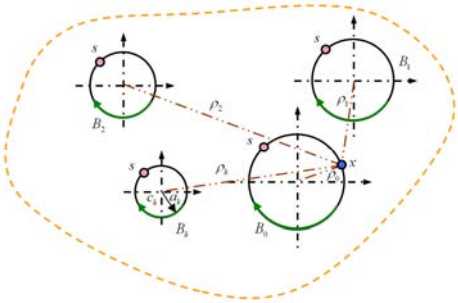

Figure 2 An adaptive observer system.

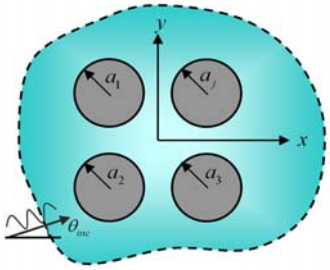

Figure 3(a) Water wave problem with multiple circular cylinders

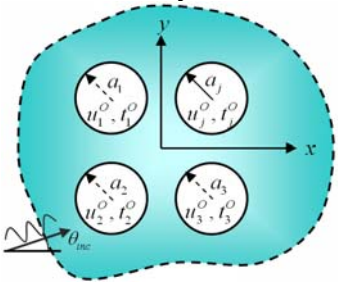

Figure 3(b)An infinite domain with multiple cylinders subject to incident water wave

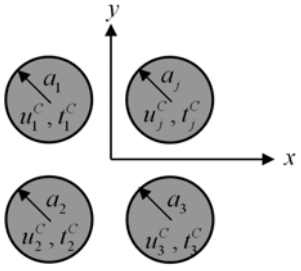

Figure 3(c) An interior Helmholtz problem for each circular cylinder

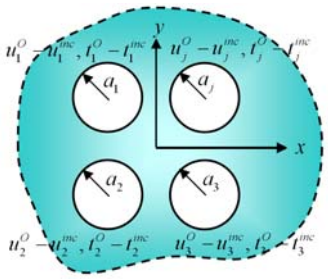

Figure 3(d) An exterior Helmholtz problem in an infinite domain

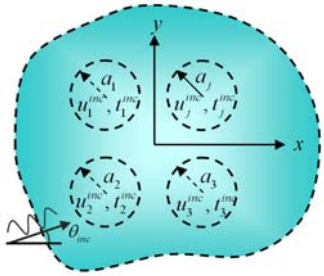

Figure 3(e) An infinite domain subject to the incident water wave

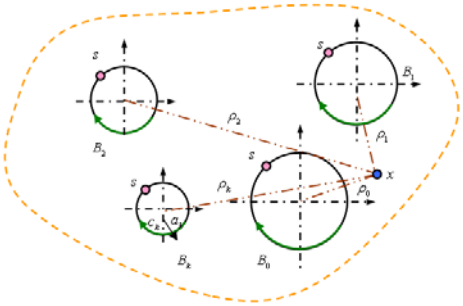

Figure 4 Sketch of the BIE for the domain point

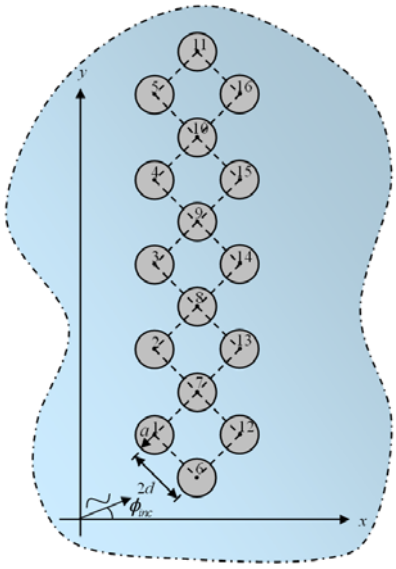

Figure 5 Configuration of sixteen cylinders

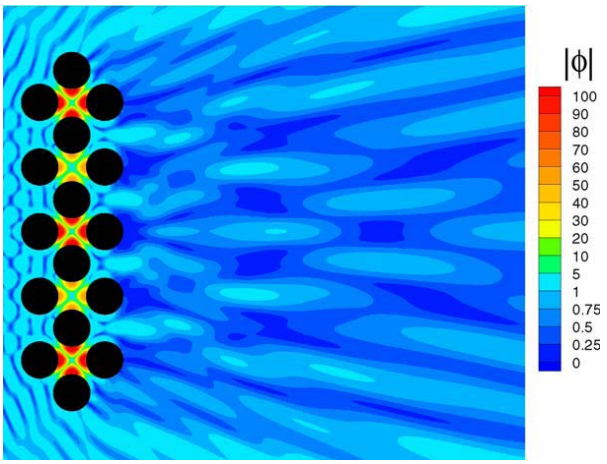

(a) Contour plot by Duclos and Clèment [17].

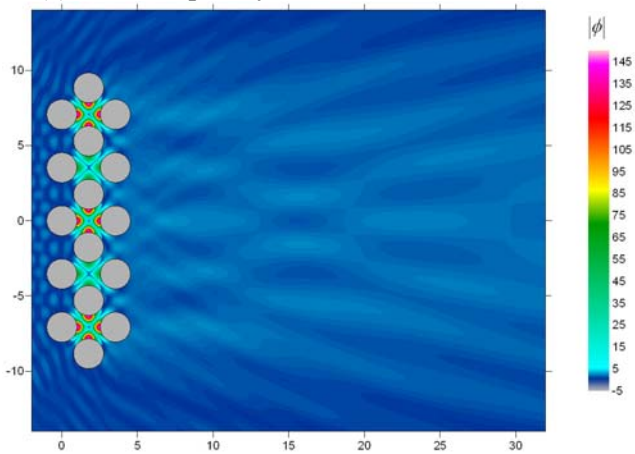

(b) Contour plot by using the present method (M=20)

Figure 6 Near-trapped mode for the ordered pile array at ka=4.08482 (a/d=0.8, G=0.0, M=20, $\tau = 0.0$)

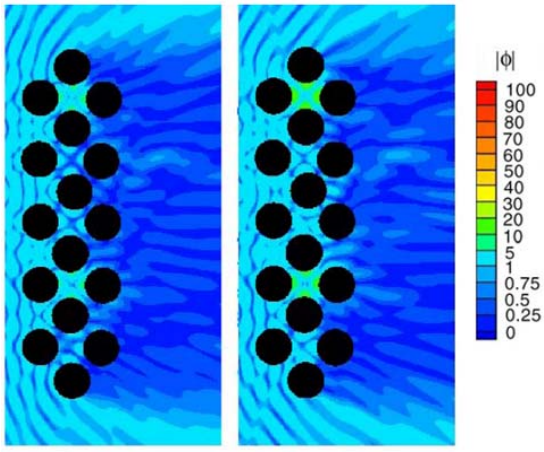

(a) Random case 1 (b) Random case 2

Figure 7 Suppression of near-trapped modes by using disorder [13] ($\tau = 0.1$).

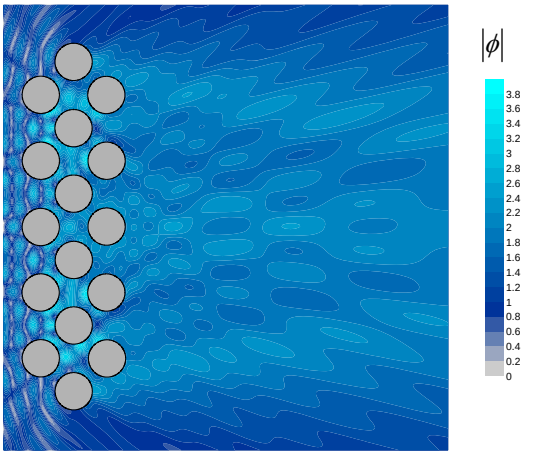

Figure 8 Suppression of near-trapped modes by using disorder. (a/d=0.8, M=20, $\tau = 0.1$)

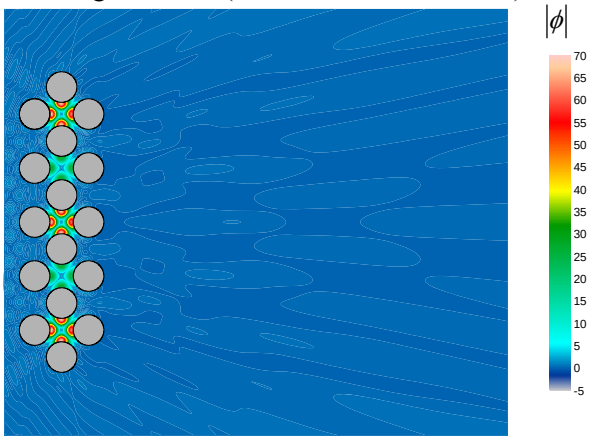

Figure 9 Contour plot of the maximum free-surface elevation amplitude for porous cylinders (a/d=0.8, G=1.0, $\tau = 0$, M=20)

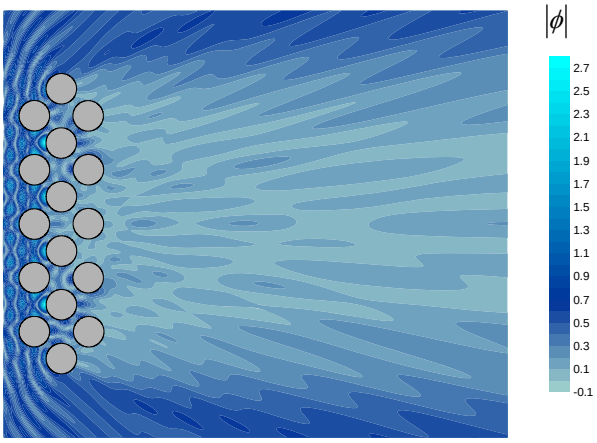

Figure 10 Contour plot of the maximum free-surface elevation amplitude for the disorder and porous cylinders (a/d=0.8, G=1.0, $\tau = 0.1$, M=20)